IL NUOVO CIMENTO **47 C** (2024) 269
DOI 10.1393/ncc/i2024-24269-6

COMMUNICATIONS: SIF Congress 2023

SYNCT: PET-driven SYNthetic control CT generation for treatment monitoring in proton therapy

M. MOGLIONI ([1])([2])([*])

([1]) *INFN, Branch of Pisa - Pisa, Italy*
([2]) *Department of Physics, University of Pisa - Pisa, Italy*

received 30 January 2024

Summary. — Proton therapy (PT) offers tumour treatments with highly conformal depth-dose distributions and less damage nearby healthy tissues over photon beam therapy. However, PT is sensitive to patient-specific anatomical variations which may lead to severe dose deviations. A control CT is generally prescribed to check the patient's morphology. Treatment verification systems such as in-beam Positron Emission Tomography (IB-PET) are desirable to avoid the delayed detection of anatomical variations during PT treatments. However, the interpretation of the PET monitoring data is still a subject of research since PET does not offer a direct representation of the disease progress as a control CT does. The SYNCT project aims to overcome this issue by using Neural Networks (NN) to produce synthetic control CT (sCT) images which can provide a non-invasive and interpretable picture of the anatomical variations in the patients. We studied the feasibility of sCT production with MC simulations. The output of our NN, a Vision Transformer, correctly produced the sCTs, which were compared with the ground truth across multiple similarity metrics. This work can be a highly valuable tool in adaptive PT.

1. – Introduction

Proton therapy allows for a precise and targeted dose to be delivered to the tumour volume and a better sparing of healthy tissues compared to conventional radiation therapy [1, 2]. However, it is hindered by anatomical changes that may arise during the treatment course. In common clinical practice, a control Computed Tomography (CT) is generally prescribed and acquired during the second or third week of treatment. This CT is used to check the patient morphology, by comparing it with the planning CT, which is instead acquired before the start of the therapy and used to plan the treatment. Despite that, critical issues remain when to correctly prescribe the control CT acquisition, since no information regarding the delivered dose during the treatment is available [3, 4].

([*]) E-mail: martina.moglioni@phd.unipi.it

Image guidance technologies are essential to provide accurate information on the irradiated volume and promptly intervene if anatomical changes occur. Cone Beam CT (CBCT), despite the lower resolution compared to conventional CT scans, rapidly becoming common in clinical facilities also thanks to the help of Artificial Intelligence (AI) [5]. However, these scans have inherent radiation risks and require careful consideration. Moreover, they can represent a burden to the patient due to repositioning and long time of acquisition [5-7].

In-beam Positron emission tomography (IB-PET) represents one of the most widely investigated non-invasive imaging techniques for *in-vivo* proton therapy monitoring [8-10]. With IB-PET, data are acquired during or immediately after irradiation inside the treatment room, avoiding additional time for the treatment and patient repositioning. Recent papers have shown the possibility of detecting anatomical changes utilizing analytical methods applied to the INSIDE IB-PET data acquired during proton therapy treatments at CNAO [11-14]. However, the lack of a direct anatomical representation in IB-PET images is still a critical issue.

The SYNCT project aims to overcome this limitation using AI techniques to create sCT images, thus providing direct anatomical information during the treatment [15-17]. This paper presents a feasibility study carried out in the project framework. The study is based on planning CT scans and MC simulations of the spatial coordinates of the annihilations that occurred within six minutes from the start of the treatment (called activity maps, AMs). A Vision Transformer (ViT) was built and fed with the planning CT and the simulated AMs from two different fractions of treatments, A and B, corresponding to six head and neck (H&N) proton-treated patients at CNAO. These data were used to produce the sCT corresponding to fraction B of the treatment.

2. – Materials and methods

For each of the six patients included in this study, both the planning CT and the control CT were available. The AMs fractions were obtained with a dedicated FLUKA-MC simulation tool. We obtained the AM_A using the planning CT. It corresponds to the reference AM, *i.e.*, patient anatomy at the beginning of the treatment course. The AM_B, instead, is obtained by using the control CT, where morphological changes can be present. We, at the moment, used the AMs instead of IB-PET data to assess the feasibility of the study, since AMs do not present limitations of instrumentation and reconstruction, as can be seen in fig. 1. We then post-processed these data to correctly create and increase the size of the training and test set for the NN. In particular:

1) For each patient we simulated separately each field of irradiation (angle of delivered dose). In the treatment plan, three irradiation fields at various angles were prescribed for all patients, except for one with only two irradiation fields. Thus, based on the number of irradiation fields, number of planning CTs (6) and control CTs (6) we obtain 17 AM_A and 17 AM_B.

2) For one patient, we also included in the dataset a set of 5 artificially modified CTs, each mimicking an increasing amount of air in the sinus cavity [14], leading to 15 additional AM_B.

3) All the 2D slices in each view (axial, coronal, sagittal) for each 3D image (CT and AMs) were used.

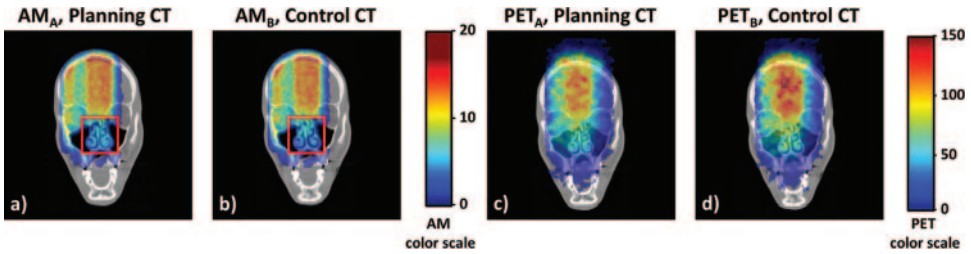

Fig. 1. – (a), (b): slice of the planning and control CT with overlayed the corresponding AMs. In the red box, the morphological change (very small, just a tiny empty of the sinus) is highlighted. (c), (d): the same slice but now with the corresponding IB-PET images. The activity present outside the patient is an example of the limitations present in IB-PET data.

4) We divided each slice into other 100 images (patches), of size 100 × 100, by randomly selecting 100 different centers in the slice.

5) We also used data augmentation techniques (Gaussian filters and random rotations) to increase the dataset.

Then a pre-trained ViT model, introduced in [18] was used [19]. In our architecture, we utilized two instances of the model, one for processing the CT data patch, and the other one for the two AMs patches. For each patch we:

1) Utilized the last attention layer thus obtaining a vector representation of the images.

2) Utilized max pooling layer to reduce the dimension of the vector.

3) Processed this vector with a series of linear layers, with LeakyReLU as activation function, and dropout layers.

4) Resampled the vector in a 100 × 100 image representing the sCT patch.

We utilized the leave-one-out cross-validation strategy to train and test the network. As a result, we evaluated the model performance for each patient included in the study.

2˙1. *Evaluation of the sCT produced.* – To establish if the sCT produced is a valid representation of the ground truth (the control CT) we opted to use the Structural similarity index metric (SSIM) and the Mean Absolute Error (MAE), widely used in literature [20, 21].

We utilized such figures of merit and then compared our results to the others presented in the following works [22-27] regarding AI-driven techniques to obtain sCT in proton therapy for H&N cancer patients using CBCT data. From our investigation, the range values reported in the cited works for the specified figures of merit are as follows: the MAE spans from 13 HU to 87 HU and the SSIM ranges from 0.90 to 0.93.

3. – Results

In fig. 2 we report an example of sCT obtained with our model. The match between the sCT (c) and the real control CT (b) is visible. We can see a blurring in the sCT,

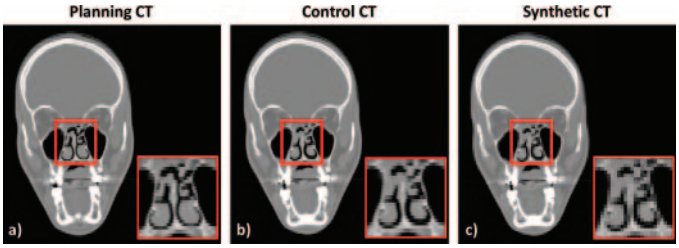

Fig. 2. – Same slice in the (a) planning, (b) control and (c) synthetic CT for one patient included in the study. The red box highlights the region of morphological change.

compared to the control CT. The blurring is more visible in the bottom right images. Despite that, the morphological change is reconstructed well by our model.

Utilizing our model, the range values for the MAE and SSIM in the skin region correspond to: the MAE varies between 9 HU and 26 HU, while the SSIM ranges from 0.87 to 0.96. It is important to note that these values are derived through the application of a leave-one-out cross-validation strategy, representing the minimum and maximum values obtained across all patients. The reported values encompass the full spectrum of performance, reflecting the variability observed in our model.

Our results lie in the range of those reported in the literature [22-27] (MAE: 13–87 HU, SSIM: 0.90–0.93). Notably, our model demonstrates exceptionally promising outcomes with lower MAE values compared to those of the literature. This reduction in MAE signifies decreased errors and a more indistinguishable representation of Hounsfield Units (HU) in the sCT and real control CT images. Furthermore, the SSIM values underscore the superior performance of our model, surpassing those found in the literature. This shows the ability of our model to reproduce structures in the skin region in the generated sCT images.

4. – Discussion

In this study, we employ vision transformers to seamlessly merge information derived from planning CT images and the interfractional activity of β^+ emitters (AMs) created by the beam in six proton-treated patients, facilitating the accurate generation of synthetic CT (sCT) images. Figure 2 shows the almost perfect match between the obtained sCT (c) and the corresponding real control CT (b). Additionally, we assessed the model's accuracy using the metrics widely used in the literature: the MAE and the SSIM. The results, corresponding to a MAE and SSIM ranking from 9 HU to 26 HU and from 0.87 to 0.96, respectively, demonstrated performance levels comparable to or slightly better than those reported in the literature (MAE: from 13 HU to 87 HU and SSIM: from 0.90 to 0.93). Based on these considerations, we assert that our model accurately reproduces sCT images from activity data, confirming the feasibility of our approach.

However, a few observations can be made. First, in fig. 2, the smaller images within the red contour highlight the sinus area, revealing a subtle emptying of the cavity. Comparing image c) with image b), we can notice an increase in blurring and a decrease in anatomical details. The sCT sinus cavity exhibits a slight graininess, which could potentially impact clinical tasks like contour segmentation and the extraction of sinus shape. However, it is out of our scope: our sCT serves as a hint for medical personnel to decide when to correctly prescribe the control CT acquisitions.

Second, it's important to acknowledge the limited amount of data and the focus on only one anatomical district (H&N). While this limitation may not compromise the quality of the generated sCT, it could affect the generalization of the model to diverse anatomical regions. Future research will include monitoring PET data of various anatomical regions and pathologies to enhance model validity and mitigate overfitting. Despite these limitations, this constraint does not compromise the method's inherent validity.

Lastly, comparing our results to those presented in the literature is challenging. Existing studies lack investigations into interfractional morphological changes, and the input data in these studies typically consist of CBCT or MRI images. These images contain a higher amount of anatomical information and a superior spatial resolution compared to our dataset, making direct comparisons difficult. Our model has the potential to be used as a pre-trained model and then further trained on IB-PET data, which, based on previous works [11-14], contains sufficient information about interfractional changes.

5. – Conclusion

This study demonstrated that planning CT scans and simulated activity of β^+ emitters are sufficient to generate high-quality sCT using AI techniques. The sCTs generated by our ViT model demonstrate good agreement with the expected control CT, as confirmed by the values of metrics of similarity, which are comparable or superior to those reported in the literature. This work paves the way to enabling a non-invasive powerful tool for online adaptive proton therapy monitoring with IB-PET data.

* * *

This research has received funding from the Tuscany Region under POR FSE 2014-2020 project SYNCT CUP I55F21002760008, and INFN. The author also acknowledges Prof. Giancarlo Sportelli (P.I. of the SYNCT project) and Dr. Pietro Carra for collaborating in the data analysis and drafting of the manuscript.

REFERENCES

[1] Durante M. and Loeffler J., *Nat. Rev. Clin. Oncol.*, **7** (2010) 37.
[2] Paganetti H., *Proton Therapy Physics* (CRC Press) 2012, https://doi.org/10.1201/9780367803551.
[3] Albertini F. *et al.*, *Br. J. Radiol.*, **93** (2020) 20190594.
[4] Kraan A. C. *et al.*, *Int. J. Radiat. Oncol. Biol. Phys.*, **87** (2013) 888.
[5] Alaei P. and Spezi E., *Phys. Med.*, **31** (2015) 647.
[6] Mathieu D. *et al.*, *J. Med. Imaging Radiat. Oncol.*, **61** (2017) 543.
[7] Li Gang, *Imaging Sci. Dent.*, **43** (2013) 63.
[8] Parodi K. and Polf J., *Med. Phys.*, **45** (2018) e1036.
[9] Sportelli G. *et al.*, *Phys. Med. Biol.*, **59** (2013) 43.
[10] Enghardt W. *et al.*, *Nucl. Instrum. Methods Phys. Res.*, **525** (2004) 284.
[11] Moglioni M. *et al.*, *JINST*, **18** (2023) C01001.
[12] Moglioni M. *et al.*, *Front. Oncol.*, **12** (2022) 929949.
[13] Fiorina E. *et al.*, *Front. Phys.*, **8** (2021) 578388.
[14] Kraan A. C. *et al.*, *Med. Phys.*, **49** (2022) 23.
[15] Moglioni M. *et al.*, *Feasibility study of synthetic CT image generation from in-beam PET in hadron therapy*, in *NSS/MIC 2022 IEEE Nuclear Science Symposium and Medical Imaging Conference, 5–12 November 2022* (IEEE) 2022, https://doi.org/10.1109/NSS/MIC44845.2022.

[16] Moglioni M. *et al.*, *SYNCT: PET-driven SYNthetic control CT generation for treatment monitoring in proton therapy*, presented at *SIF 109th Congress* (2023).
[17] Moglioni M. *et al.*, *Monte Carlo feasibility study of PET driven synthetic CT imaging for disease monitoring in proton therapy*, in *Proceedings to the 61st Annual Conference of the Particle Therapy Cooperative Group, 10 June–16 June 2023*, *Int. J. Part. Ther.*, **10** (2023) 118, P328 (Elsevier) 2023, https://doi.org/10.14338/IJPT-23-PTCOG61-10.2.
[18] Wu B. *et al.*, Visual Transformers: Token-based Image Representation and Processing for Computer Vision, arXiv:2006.03677 (2020).
[19] Shamshad F. *et al.*, *Med. Image Anal.*, **88** (2023) 102802.
[20] Peng H. *et al.*, *IEEE Trans. Radiat. Plasma Med. Sci.*, **7** (2023) 213.
[21] Spadea M. F. *et al.*, *Med. Phys.*, **48** (2021) 6537.
[22] Thummerer A. *et al.*, *Phys. Med. Biol.*, **65** (2020) 235036.
[23] Zhiwen L. *et al.*, *J. Radiat. Res. Appl. Sci.*, **17** (2024) 100809.
[24] Lalonde A. *et al.*, *Phys. Med. Biol.*, **65** (2020) 245022.
[25] Kurz C. *et al.*, *Phys. Med. Biol.*, **64** (2019) 22504.
[26] Zhang Y. *et al.*, *Technol. Cancer Res. Treat.*, **21** (2022) 15830338221085358.
[27] Chen X. *et al.*, *Front. Oncol.*, **12** (2022) 988800.